Undergraduate Journal of Experimental Microbiology and Immunology (UJEMI) Vol. 29:1-11

Steps Towards Unraveling the Driving Force of BrkA Passenger Domain Translocation: The Role of Passenger Domain Length in Secretion Efficiency

Madeleine Dunsmore, Olivia Kwon, Emily Moffat

Department of Microbiology and Immunology, University of British Columbia, Vancouver, British Columbia, Canada

SUMMARY Autotransporters are a unique type of secretion system utilized by gram-negative bacteria to secrete proteins across the bacterial outer membrane. Specifically, *Bordetella pertussis* employs the BrkA autotransporter to provide resistance to host serum killing and to mediate host cell surface attachment. BrkA protein structure has been characterized with a signal peptide, a passenger domain which is secreted, and a translocation domain that remains anchored in the outer membrane. The translocation of the passenger domain requires energy; however no ATP hydrolysis or proton gradients are involved. Previous literature has proposed a model for autotransporter passenger domain translocation in which an increase in free energy due to the disruption of the passenger's hydrating shell during translocation drives its secretion. However, no exact mechanism has been described for the driving force of BrkA translocation. Therefore, this study aimed to explore the potential application of the free energy model on BrkA passenger domain translocation by creating three *brkA* constructs, each with different passenger domain lengths, and measuring their relative surface display efficiencies. Various lengths of BrkA passenger domain were created with primers designed to amplify only desired regions of the *brkA* gene, while intentionally removing unamplified sequences. After confirming correct deletions via restriction enzyme digest and Nanopore sequencing, western blotting was used to investigate BrkA expression. After several attempts, BrkA expression from plasmid constructs with altered passenger domains was not detected. Despite difficulties elucidating the exact cause of this unsuccessful detection, this paper sets a foundation for understanding the importance of the passenger domain in BrkA stability and expression. Understanding the driving force of BrkA translocation may provide insight into the mechanism of bacterial pathogenesis and potentially lead to new therapeutic targets.

INTRODUCTION

Bacterial secretion systems are essential in gram-negative bacteria for various important functions ranging from surface attachment and transport across the cell envelope to motility and pathogenesis (1, 2). Classified from Type 1 to Type 11, bacterial secretion systems use numerous unique mechanisms to transport proteins across the bacterial inner and outer membranes (3–5). Among the different types, Type V Secretion Systems (T5SS), also known as autotransporters, are exclusive in their ability to insert themselves into the bacterial outer membrane (OM) and simultaneously transport their own proteins and other proteins across the OM (1–3, 6). The *Bordetella* resistance to killing A (BrkA) protein is an autotransporter in the autotransporter-1 subfamily of T5SS and functions as a virulence factor for *Bordetella pertussis*, the etiological agent of whooping cough (6, 7). By providing resistance to complement-dependent killing by host serum and mediating surface attachment, the BrkA system is a key component of *B. pertussis* pathogenesis (6, 8).

The autotransporter system is known as the simplest bacterial secretion system, as it is made up of a single polypeptide chain (2, 9, 10). Similar to other autotransporters, BrkA is initially translated as a precursor with a molecular weight of 103 kDa (6, 11). It is then subjected to proteolytic cleavage, leading to the formation of three distinct domains: a 42-amino-acid N-terminal signal peptide, a 73 kDa passenger domain and a 30 kDa C-terminal translocation domain (6, 11, 12). The translocation domain forms a conserved β-barrel pore that inserts itself into the bacterial OM, as required for translocation (11, 13). Upon β-barrel

Published Online: September 2024

Citation: Dunsmore, Kwon, Moffat. 2024. Steps towards unraveling the driving force of BrkA passenger domain translocation: The role of passenger domain length in secretion efficiency. UJEMI 29:1-11

Editor: Shruti Sandilya and Ronja Kothe, University of British Columbia

Address correspondence to: https://jemi.microbiology.ubc.ca/

formation and insertion, the passenger domain is translocated through the β-barrel and remains anchored to the membrane after translocation (14, 15).

Studies have shown that the translocation of the BrkA passenger domain occurs without ATP hydrolysis or a proton gradient (5, 14–16). It is also known that the transport β-barrel channel is too narrow to allow for a folded passenger domain to translocate through, meaning the passenger must translocate in an unfolded—at least partially—state (15, 16). However, the exact mechanism or driving force that allows this translocation is unknown. Residue substitution experiments have led to development of a model in which secretion of the passenger domain is driven by the increase in system stability that occurs during folding of the passenger domain at the cell surface (14, 15). Furthermore, a study by Pang *et al*. described an energetic model of pertactin, an autotransporter from *B. pertussis* in which the folding of its passenger domain during secretion increases the free energy of the system (17). They present a specific model called the vectorial folding pathway where in the bacterial periplasm, a hydrating shell protects the passenger domain from spontaneously folding into its secondary protein structure (17). As the passenger domain passes through the OM, it forms a β-helix structure, resulting in its hydrating shell being shaken off (17). The shaken off water molecules increase the overall entropy of the system, serving as a driving force for passenger domain translocation through the OM (17).

The BrkA autotransporter has been previously used to secrete heterologous proteins by substituting parts of the passenger domain with genes encoding proteins such as proteases biocatalysts, single-chain antibodies, and green fluorescent protein (18, 19, 19). However, the measurement of exogenous protein secretion by BrkA has not been characterized. This study aimed to determine how much of the native passenger domain is required for successful protein secretion using the BrkA autotransporter, and to optimize secretion efficiency of exogenous proteins inserted within the passenger domain. Based on previous research, we hypothesized that relatively longer passenger domains will secrete through the OM more readily because they will shake off more water molecules while folding outside the cell, thereby creating a more positive entropy change in the system compared to their shorter counterparts. Investigating the connection between the length of the native passenger domain and the secretion efficiency of the BrkA system will provide a more comprehensive understanding of the driving force of BrkA passenger domain secretion. Optimizing the process of secreting exogenous proteins using BrkA may support various efforts in biotechnology to leverage autotransporter systems for protein engineering and therapeutic applications.

METHODS AND MATERIALS

Cell culture, strains and plasmids. All bacterial strains used in this study were obtained from the Department of Microbiology and Immunology at the University of British Columbia. pDO-6xHis6935 (pENS) containing NEB 5-alpha cells were constructed by Goh *et al.* (2023). Liquid cultures were all grown in Luria Bertani medium supplemented with 50 mg/mL of ampicillin.

Luria Bertani (LB) and ampicillin selective media preparation. LB broth and agar plates were made according to the protocol by Tu *et al*. (20). A sterile ampicillin working stock was prepared by filter sterilization of a 50 mg/mL dissolved solution. LB broth and agar plates were supplemented with ampicillin to a final concentration of 50 µg/mL. All overnight cultures prepared for this study were grown at 37°C in 5 mL of LB supplemented with 5 µL of stock ampicillin where needed.

PCR primer design. Using AlphaFold, BrkA was visualized to select three different non-β-helix structural locations that primers could bind to and amplify only the desired regions, thereby creating intentional deletions (Figure 1D). DNA primers were designed using SnapGene to create the directed deletions resulting in a long, medium, or short passenger domain while inserting a restriction enzyme cut site in frame with the *brkA* sequence (Figure 1C). A total of four primers were designed to amplify the three constructs; one forward primer and three different reverse primers that would facilitate the different deletions (Table 1). Each primer was designed with a 5’ overhang containing a ScaI restriction enzyme cut site. These

overhangs were ensured to be complementary so that upon annealing of forward and reverse primers, the overhangs would introduce a functional cut site.

TABLE. 1 Primer information for pENS backbone amplification with different length *brkA* passenger domain deletions and ScaI restriction site insertion.

Primer	Sequence	Tm	Ta	GC
F	5' - agtactGTCCCGGTGGTCGAACTCT - 3'	61°C	56°C	60%
R1 (pMOE1)	5' - agtactAACACGCTCATTGCAGTCTTTGA - 3'	58°C	53°C	43%
R2 (pMOE2)	5' - agtactGAGCCGCAGTCCGGCTCC - 3'	64°C	59°C	78%
R3 (pMOE3)	5' - agtactGAGGCCTCTTACAAGACCCTGA - 3'	57°C	52°C	55%

pENS plasmid isolation. A culture of NEB 5-alpha *Escherichia coli* cells containing pENS plasmids was prepared by overnight incubation at 37°C in LB supplemented with ampicillin (50 µg/mL). The plasmids were extracted and purified using the manufacturer protocol for purification of plasmid DNA from EZ-10 Spin Column DNA Cleanup Miniprep Kit (BioBasic; Cat.# BS614). Plasmid concentration and purity were evaluated with NanoDrop™ 2000 Spectrophotometer (ThermoFisher) and stored at -20°C.

Polymerase Chain Reaction (PCR) amplification. PCR reagents, reagent volumes and final concentrations were based on the New England Biolabs Q5® Site-Directed Mutagenesis Kit (E0554). Using a separate T100 Thermal Cycler (Bio-Rad) for each reaction, the reaction tubes underwent an initial denaturation at 98 ºC for 30 seconds. Then, they were subjected to 25 cycles of denaturation (98 ºC for 10 seconds), 30 seconds of annealing (68ºC for R1, 71ºC for R2, 69ºC for R3), and extension for a total of 3.5 minutes for 7 kb (72ºC for 30 s/kb). Q5-optimized annealing temperature of primers were determined using NEBaseChanger™. Lastly, the final extension was at 72ºC for 2 minutes and held at 4ºC until recovery.

Agarose gel electrophoresis of PCR products. A 1% agarose gel was prepared with 1g of agarose added to 100 mL of 1X TAE buffer and was dissolved with a 30 second interval microwave exposure. 5 µL of 20,000X RedSafe™ Nucleic Acid Staining Solution (iNtRON Biotechnology) was added to the dissolved solution and mixed. In the first lane, 5 µL of O'GeneRuler DNA Ladder Mix (Thermo Scientific Cat.#SM1173) was added. 3 µL of PCR amplification products were each mixed with 0.5 µL of 6X DNA loading dye (New England BioLabs; Cat.# B7024S) and loaded into the gel. The loaded samples and controls were run at 110V for 60 minutes and imaged using ChemiDocMP imaging system (Bio-Rad) on the GelRed setting.

Kinase, Ligase and Dpnl (KLD) reaction and transformation. KLD reaction and transformation of NEB 5-alpha Competent *E. coli* cells of each PCR amplification product were conducted using materials and protocol from the New England Biolabs Q5® Site-Directed Mutagenesis Kit (E0554). For concentrated plating of cells, Q5® ligated products were centrifuged for 2 minutes at 10 000 RPM, resuspended in 100 µL of Super Optimal broth with Catabolite repression (SOC) and plated on LB agar plates supplemented with 50 µg/mL of ampicillin. Transformed cells were grown overnight at 37°C.

Preparation of chemically competent UT5600 *E. coli* cells. A culture of UT5600 *E. coli* cells was prepared by overnight incubation at 37°C in LB supplemented with ampicillin (50 µg/mL). 1 mL of overnight culture was added to 100 mL of LB broth and shaken at 37°C until OD_{600} = 0.4. Upon reaching this cell density, the culture was set on ice for 10 minutes then centrifuged at 4000 g for 5 minutes at 4°C. Cells were resuspended in 50 mL of ice-cold 60 mM $CaCl_2$ solution (0.67 g $CaCl_2$ in 100 mL dH_2O) and placed in an ice bath for 30 minutes. The cell suspension was centrifuged at 4000 g for 5 minutes at 4°C and resuspended in 5 mL of ice-cold $CaCl_2$ + 15% glycerol (4 mL of 100% glycerol, 25 mL of dH_2O and 0.17g $CaCl_2$,). 50 µL aliquots were dispensed and stored at -70°C for future use.

ScaI restriction enzyme digest and gel electrophoresis. Overnight cultures of transformed NEB 5-alpha cells for each Q5 product were grown at 37°C in 5 mL LB supplemented with

5 µL stock ampicillin (50 mg/mL). Plasmids from each culture were extracted using the same method mentioned previously. Each plasmid DNA concentration was determined by NanoDrop™ 2000 Spectrophotometer (ThermoFisher) and used to calculate the appropriate volume of plasmid required for 1 µg of plasmid DNA. In each reaction microfuge tube, 5 µL of 1X rCutSmart Buffer (New England BioLabs; Cat.# B6004S), 1 µg of plasmid DNA (autoclaved dH_2O for negative control and pENS for positive control), and 1 µL of ScaI-HF® (New England BioLabs; Cat.# R3122S) enzyme were added, and filled with dH_2O to a total volume of 50 µL. These reaction tubes were incubated at 37°C for 15 minutes and heat inactivated at 65°C for 20 minutes. Following this restriction enzyme digest, another 1% agarose gel electrophoresis was performed under the same protocol mentioned above. Unused plasmids were stored at -20°C.

Nanopore sequencing via Plasmidsaurus. 20µL of each purified plasmid normalized to 30 ng/µL with an elution buffer (10 mM Tris, pH 8.5) was added to labeled PCR strip tubes. A total of three samples (one for each construct) were sent to Plasmidsaurus for Nanopore sequencing.

Heat shock cell transformation. 150 ng of previously purified plasmid constructs (pMOE1, pMOE2, and pMOE3) were each added to 50 µL of competent UT5600 *E. coli* cells in appropriate volumes and incubated on ice for 30 minutes. The mixtures were then transferred to a 42°C water bath for exactly 2 minutes followed by a 5-minute incubation on ice. Finally, the cells were incubated at 37°C for one hour, with 1 mL of LB added to each mixture. Cells were spread plated on one LB agar plate and one ampicillin-supplemented LB agar plate. Plates were incubated overnight at 37°C and recovered the following day.

IPTG induction and whole cell lysis for protein extraction. Note that for untransformed *E. coli* cells, no ampicillin was added throughout the procedure. 20 µL of each overnight culture of pMOE1, pMOE2, and pMOE3, positive and negative controls were added to 2 mL of LB and 2 µL of stock ampicillin and grown for 3 hours at 37°C. A stimulation solution containing 1 mL of LB, 1 µL of ampicillin and 20 µL of 1 mM isopropyl β-D-1-thiogalactopyranoside (IPTG) was pre-warmed at 37°C and added to each culture, bringing the final concentration of IPTG to 0.5mM. Cultures were incubated for another 3 hours at 37°C. IPTG-stimulated cells were normalized to an OD_{600} reading of 0.5 using fresh LB. 100 µL of normalized cultures were centrifuged at 12 000 RPM for 2 mins and resuspended into 75 µL of Laemmli buffer with 5% β-mercaptoethanol (BME). Then they were subjected to 5 minutes of boiling at 95°C in a heat block and stored at -20°C.

SDS-PAGE. A 12% acrylamide gel was made using the TGX™ FastCast™ Acrylamide Starter Kit (Bio-Rad Cat.#1610175). 10 µL of experimental cell lysates, 6 µL of PageRuler™ Plus Prestained Protein Ladder (BioRad Cat.#1610375) and controls were loaded onto the gel. Remaining wells were filled with 6 µL of Laemmli buffer with 5% BME. Gel was run at 150V for 50 minutes and imaged using the ChemiDoc Imaging System (Bio-Rad).

Western blot. Resolved proteins were transferred to a PVDF membrane using the Trans-Blot® Turbo mini transfer pack (Bio-Rad), following manufacturer instructions. The membrane was blocked with 5% BSA in TBS-T for 1 hour at room temperature, followed by brief washes with TBS-T. Then a primary antibody solution (5 µL of anti-6xHis antibody (Invitrogen) in 15 mL of 1% BSA in TBS-T) was added to the membrane and incubated overnight at 4°C on an orbital shaking incubator. The following day, the membrane was washed with TBS-T and incubated in a secondary antibody solution (1.5 µL of HRP-conjugated goat anti-mouse IgG antibody (Invitrogen) in 15 mL of 1% BSA in TBS-T) for 1 hour at room temperature. Lastly, the membrane was washed three times with dH_2O, three times with TBS-T and three times with TBS, followed by the addition of a chemiluminescent detection solution (3.5 mL of luminol and 3.5 mL of peroxide) and imaging using the ChemiDoc MP Imaging System (Bio-Rad).

RESULTS

Our experimental workflow involved using Q5 to create deletions within the *brkA* passenger using our designed primers, via exclusion of the region between the forward and reverse primers during amplification. Figure 1A-B demonstrates the intended experimental BrkA proteins with generated passenger deletions based on our generated constructs.

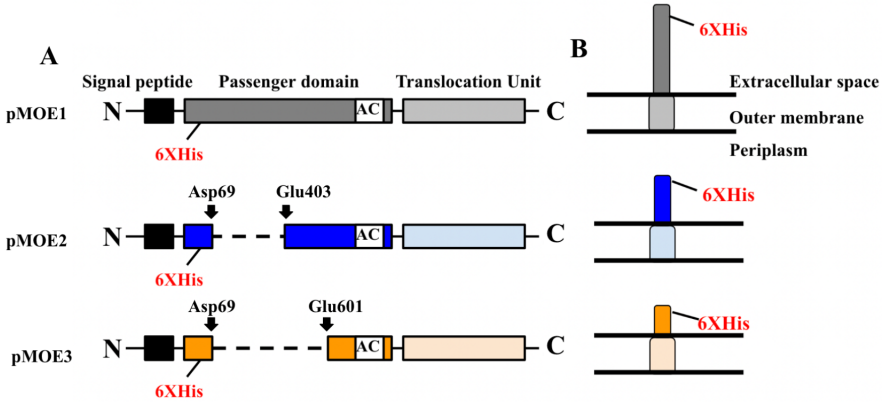

FIG. 1 Schematic of theoretical constructs. (A) Desired constructs, referred to as pMOE1 (long passenger), pMOE2 (medium passenger), and pMOE3 (short passenger), protein constructs annotated with expected deletions within the passenger domain. Amino acids indicate the boundaries of the deletion (amino acid specified is included). (B) Model of hypothesized surface expression of BrkA from each pMOE.

Generation of passenger deletions in pMOE1, pMOE2 and pMOE3 constructs using site directed mutagenesis. As described in Figure 1, we first generated three experimental constructs of *brkA* with various lengths of the passenger domain deleted (pMOE1, pMOE2, and pMOE3) using site directed mutagenesis. Expected band sizes for each pMOE amplification reaction were calculated based on the pENS backbone size of 6945 bp (Goh *et al.*, unpublished manuscript) and engineered deletion sizes. PCR amplification yielded the expected band sizes for each pMOE with minimal non-specific banding or smearing (Figure 2A). Notably, pMOE2 had a visibly fainter band than pMOE1 or pMOE3, which is likely attributable to the higher GC content of the reverse primer used to generate pMOE2 relative to pMOE1 or pMOE3. However, because the expected band sizes were present for all three constructs, we proceeded with the subsequent KLD re-ligation reaction.

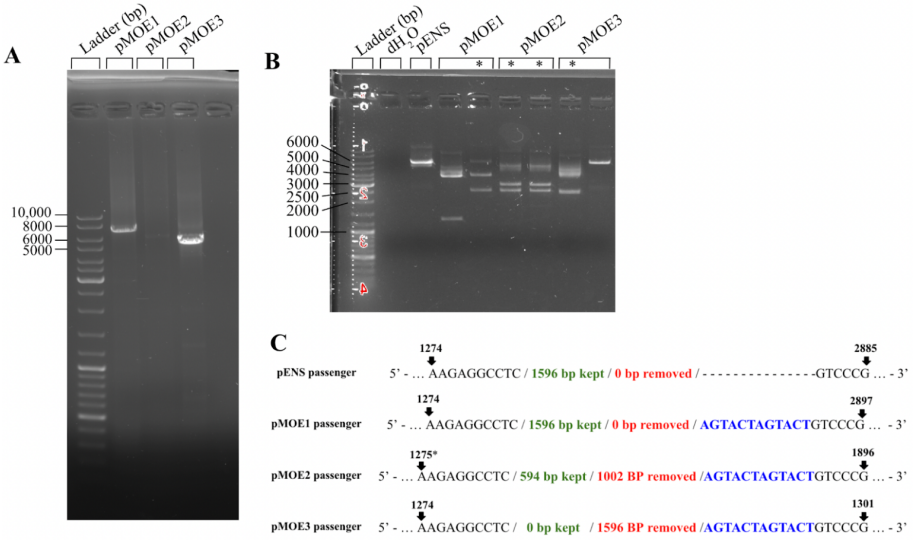

FIG. 2 Generation of pMOE1, pMOE2 and pMOE3 by Q5® site-directed mutagenesis are confirmed by restriction digest and Nanopore sequencing. (A) Q5® amplification products of pMOE1, pMOE2, and pMOE3 were run on a 1% agarose gel. Expected band sizes were 7kb for pMOE1, 6kb for pMOE2, and 5.3kb for pMOE3. No controls were run due to limited reagents. (B) ScaI restriction enzyme digest results of pMOE1, pMOE2, and pMOE3, negative control (nuclease free dH_2O), and positive control (pENS) were run on a 1% agarose gel. Asterisks indicate lanes with expected band sizes present. Expected sizes were 2.7kb and 4.2kb for pMOE1, 2.7kb and 3.2kb for pMOE2, and 2.7kb and 2.6kb for pMOE3. For each pMOE, extracted plasmid from an opaque (left) and translucent (right) colony was digested. (C) Display of relevant passenger domain regions from Nanopore sequencing (Plasmidsaurus) results aligned in SnapGene demonstrate correct deleted and adjacent upstream/downstream sequences. Green text indicates intact aligned sequences, red text indicates deletions, and blue text indicates inserted ScaI sites. Numbers indicate the position of the indicated base pair within the passenger domain. Asterisk indicates that pMOE2's initial position is 1275 instead of 1274 due to an additional inserted base at the start of the plasmid.

After transforming NEB 5-alpha *E. coli* cells with our finalized pMOE1, pMOE2 and pMOE3 constructs, we observed two distinct transformant colony morphologies—opaque and translucent. We were unsure if this morphology difference was related to *brkA* expression, therefore we proceeded to screen both morphologies for each pMOE. ScaI restriction digest was performed to screen for correctly inserted ScaI restriction sites, and correct passenger deletions within each pMOE. The restriction digest displayed expected band sizes based on the location of the newly inserted and previously existing ScaI restriction sites (Figure 2B). Given that the extracted pMOE2 from both the translucent and opaque colonies produced the expected band sizes, we concluded that the differing colony morphologies were likely unrelated to the design of our constructs. Although some non-specific banding and smearing were present, we proceeded with the plasmid samples which produced the expected band sizes and further verified these constructs via sequencing.

Nanopore sequencing by Plasmidsaurus of the promising pMOE1, pMOE2, and pMOE3 samples revealed that the exact deletions we engineered were created (Figure 2C). However, they also revealed accidental insertion of a second ScaI restriction site immediately downstream of the first (intended) ScaI site (Figure 2C). Given that this extra ScaI restriction site added 6 bp, its insertion is in frame with *brkA* and therefore should not affect expression of *brkA*. While pMOE1 and pMOE3 had the exact number of base pairs as expected after taking into account the extra ScaI site, pMOE2 had one extra base pair. Concerned with a possible frameshift mutation, we used bioinformatic tools to confirm that the extra base pair would not impact *brkA* transcription and translation. Upon further investigation, we discovered that the additional base pair in pMOE2 was inserted at the beginning of the plasmid, resulting in a sequence where a normally occurring run of 8 adenosine bases was extended to 9 adenosine bases. Taken together, the results of the Q5® amplification, restriction digest, and Nanopore sequencing confirmed production of the desired experimental constructs.

BrkA is not detected in whole cell lysates of pMOE1, pMOE2, and pMOE3 transformed UT5600 cells. After the plasmid constructs were made, the next step was to assess BrkA expression in *E. coli* derivative UT5600 cells transformed with pMOE1, pMOE2, and pMOE3. Prior to lysis, overnight cultures of each experimental sample and control were cultured with IPTG for 3 hours to induce *brkA* expression. This step was conducted because *brkA* expression has been hypothesized to be under the Lac promoter—an IPTG-inducible promoter (Haniak *et al.* 2023, unpublished manuscript). Whole cell lysates of IPTG-induced pMOE1, pMOE2, and pMOE3 transformants were resolved by SDS-PAGE and subsequently analyzed via western blotting for detection of the BrkA-associated 6xHis tag. Prior to western blotting, visualization of the whole cell lysate samples resolved using SDS-PAGE revealed the presence of resolvable protein bands in all samples (Figure S1). Since our samples contained resolvable proteins, we proceeded with a new SDS-PAGE and subsequent western blot. The blot revealed bands corresponding to the sizes of cleaved and uncleaved BrkA in the positive control, but not in the negative control or in any of the pMOE1, pMOE2, and pMOE3 transformant samples (Figure 3A). Non-specific bands were observed in each of the pMOE1, pMOE2, and pMOE3 transformant samples, although these bands were also present in the positive and negative controls and were therefore considered background signal.

This preliminary western blot included pPALMC as the only positive control and not pENS—the plasmid used to create our experimental constructs. pPALMC was used as a positive control because team 1 epsilon was able to detect BrkA by probing for its 6XHis tag. Therefore, a second western blot was performed to determine whether BrkA could be detected in the unmodified pENS plasmid backbone. In this new western blot, bands corresponding to cleaved and uncleaved BrkA were observed in the pENS sample, but not in any of the pMOE1, pMOE2, and pMOE3 transformant samples (Figure 3B). Both negative controls were devoid of BrkA banding, as expected. Interestingly, no bands corresponding to BrkA were observed in the pPALMC sample aside from a very faint band near 120kDa, although this is likely explained by low protein concentration and small loaded volume. As before, various non-specific bands were detected in each of our experimental samples but were considered as background signal due to the same banding pattern being observed in the controls.

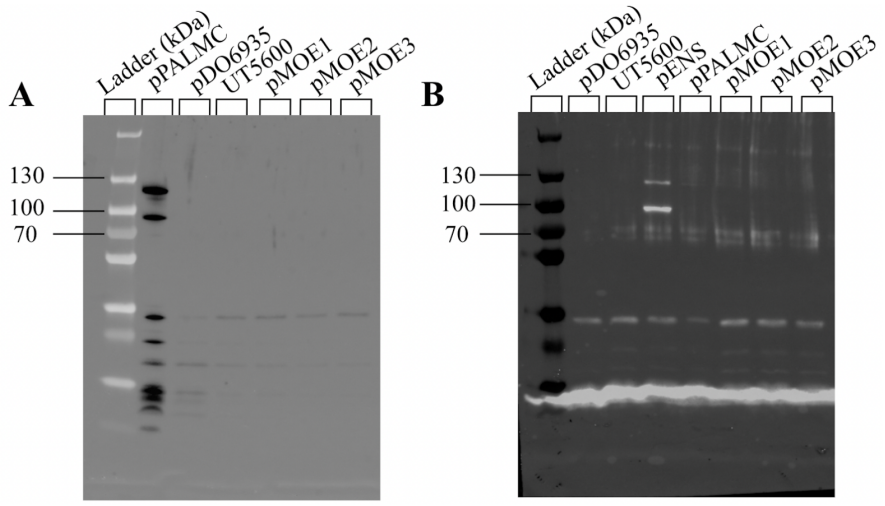

FIG. 3 BrkA-associated 6XHis tag cannot be detected in pMOE1, pMOE2 and pMOE3. Anti-6xHis western blots of IPTG-induced, whole cell lysate samples and controls in Laemmli with 5% BME. Both blots were run alongside PageRuler™ Plus Prestained Protein Ladder (BioRad) and were visualized as a composite colorimetric and chemiluminescence image. (A) The positive control was a pPALMC protein sample (donated from team 1 epsilon). The negative controls included pDO6935-containing DH5α cells and untransformed UT5600 cells. (B) Positive controls include pENS-containing NEB 5-alpha cells and pPALMC protein sample (donated from team 1 epsilon; different sample than in A). Negative controls include pDO6935-containing DH5α cells and untransformed UT5600 cells. Expected band sizes for BrkA are 103kDa for uncleaved BrkA, and 73kDa for cleaved BrkA.

DISCUSSION

In this study, we generated *brkA* constructs (pMOE1, pMOE2, and pMOE3) by deleting various lengths within the passenger domain to explore the role of passenger domain length on BrkA surface display efficiency. Restriction digest and Nanopore sequencing results indicated that our deletions were made exactly as planned in each of the pMOE plasmids (Figure 2B-C). The sequencing results revealed an unexpected second ScaI insertion immediately downstream of the intended ScaI site (Figure 2C). This can be attributed to our primer design, given that we included a 5' overhang containing the ScaI restriction site sequence on *both* the forward and reverse primers for the reaction, instead of placing the half of the respective insertion on each forward and reverse primer. Nevertheless, these extra base pairs introduced into each plasmid sequence were in frame with BrkA and were located in a non-structural region (Figure 4B). Therefore, we do not expect that this impacted BrkA expression or structure.

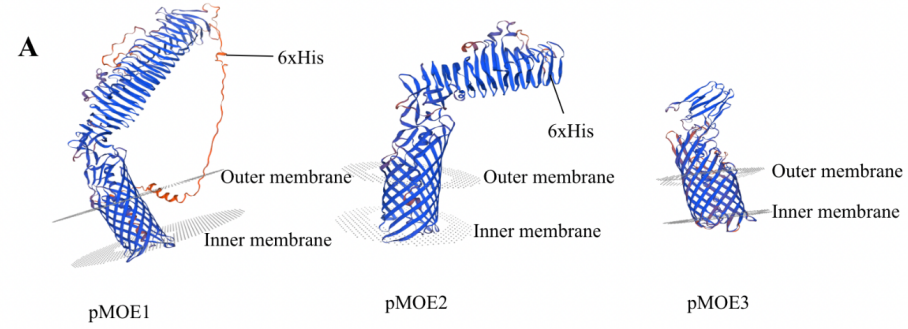

B

pENS **N - MYLD**RFRQCP / 44 amino acids / AQDAG**HHHHHHH**QEGEFD / **936 amino acids** / FHAGY**RYSF - C**

pMOE1 **N - MYLD**RFRQCP / 44 amino acids / AQDAG**HHHHHHH**QEGEFD / **940 amino acids** / FHAGY**RYSF - C**

pMOE2 **N - MYLD**RFRQCP / 44 amino acids / AQDAG**HHHHHHH**QEGEFD / **606 amino acids** / FHAGY**RYSF - C**

pMOE3 **N - MYLD**RFRQCP / 44 amino acids / AQDAG**HHHHHHH**QEGEFD / **408 amino acids** / FHAGY**RYSF - C**

FIG. 4 Predicted protein models and Expasy translated sequences of pMOE1, pMOE2 and pMOE3 proteins. (A) SWISS-MODEL generated structural models based on the translated sequences of *brkA* in pMOE1, pMOE2 and pMOE3. Locations of 6xHis tags in pMOE1-2 shown; pMOE3's generated model did not include the translated sequence's 6xHis tag. (B) Relevant translated sequence from the *brkA* open reading frame (3' to 5', ORF 2), obtained from Nanopore sequencing results of pMOE1, pMOE2 and pMOE3, the known sequence of pENS, using the Expasy Translate tool. Red text indicates the location of the 6xHis tag, blue text indicates the first and last amino acids of BrkA, demonstrating in-frame translations, and green text highlights the different number of passenger domain amino acids in each pMOE.

Upon generation of our desired constructs, we proceeded to investigate BrkA expression in pMOE1, pMOE2, and pMOE3 using western blotting of whole cell lysates probing for the 6xHis tag added to pDO6935 by Goh *et al.* (2023, unpublished manuscript) (Figure 3). Constructs were first transformed into an endonuclease-free cell line (DH5α), to screen for recircularized plasmids and increase their concentration before transforming into the final experimental system of UT5600 cells. As the pENS plasmid contains an engineered OmpT cut site at the beginning of the brkA passenger domain, using UT5600 was essential to measure BrkA secretion without the interference of OmpT cleavage (21).

Unfortunately, we were unable to detect BrkA expression from any of the pMOE1, pMOE2, or pMOE3 samples (Figure 3). Positive controls of pPALMC (generously donated by team 1 epsilon) and pENS produced expected BrkA banding, indicating that our protocols for IPTG induction, whole cell lysis for protein extraction, and western blotting were robust and conducted accurately (Figure 3). In the initial western blot (Figure 3A), the pPALMC positive control exhibited a bright signal. However, in the subsequent blot (Figure 3B), it was not as prominently detected. This variance can likely be attributed to the use of different cell lysate samples obtained from team 1 epsilon. It is plausible that the pPALMC sample in the second blot had a significantly lower concentration compared to the first, therefore resulting in its faint detection.

Moreover, an initial SDS-PAGE validated the existence of resolvable proteins in our pMOE1, pMOE2, and pMOE3 samples, implying that the failure to detect BrkA was not the result of an absence of proteins (Figure S1). Finally, ahead of our second failed western blot, we performed the IPTG induction and harvested whole cell lysates for all our samples again, suggesting that a source of error associated with sample preparation is unlikely. Taken together, we are confident that we would have detected BrkA in western blots of our pMOE1, pMOE2, and pMOE3 samples if it was being expressed and contained a functional and accessible 6xHis tag.

This conclusion led us to begin exploring potential sources of error related to BrkA expression and 6xHis tag accessibility. We began by exploring the 3D protein structure of BrkA expressed by each of our constructs to determine if there were any obvious structural issues that may have prevented the detection of the 6xHis tag during western blotting (Figure 4). This was done by translating each of our plasmid sequences using the Expasy Translate tool and generating a 3D protein model of BrkA using the corresponding amino acid sequence and Expasy's SWISS-MODEL tool (22, 23). Based on the generated models, the overall structure of BrkA from each of our constructs is similar to the native BrkA structure, aside from progressively shorter passenger domains. All of our engineered BrkA proteins retained the key structural elements, having comparable β-barrel and β-helical structures to native BrkA. This is especially true for pMOE1, since its passenger domain is near-identical to native BrkA, with only an addition of 4 amino acids in a non-structural region corresponding to the introduced ScaI sites (Figure 4B). Furthermore, the 6xHis tag in pMOE1 appears to be positioned in the correct location and orientation (Figure 4A), which should have facilitated the anti-6xHis antibody binding during the western blotting. While the 6xHis tag is incorporated within the second fold of the passenger's β-helix, given that SDS-PAGE denatures the protein structure, this should not have impacted its detection. Therefore, it is surprising that we were unable to detect pMOE1 or pMOE2 in any of our western blots. The pMOE3 model also appears to have intact structural domains, containing the expected β-helix and truncated β-barrel structures (Figure 4B). However, the model generated for pMOE3 did not include the 6xHis tag residues despite them being present in the translated sequence; the 6xHis tag is in position 60-65 of the translated sequence, however the protein model begins at the glycine residue in position 68. Assuming this model is accurate, this might reasonably explain why we failed to detect pMOE3 in any of our western blots.

Overall, based on the predicted structural models for pMOE2-3 it is not surprising that 6xHis tag detection did not occur during western blot. However, because pMOE1 was not detected despite having an ideal structure, we are hesitant to conclude that the cause for our inability to detect our plasmid constructs was solely due to structural issues in the pMOE1, pMOE2, and pMOE3 proteins.

When the structural models of BrkA from pMOE1, pMOE2, and pMOE3 failed to explain our western blot results, we hypothesized that there may have been a problem with the coding

region of *brkA* which prevented proper transcription or translation of *brkA.* To explore this possibility, we returned to the data we obtained from the Expasy Translate tool to examine the open reading frame of *brkA* in each of our constructs relative to the open reading frame of *brkA* in the unmodified pENS plasmid (22). This analysis confirmed that our deletions, ScaI site insertions, and even the unindented extra adenosine base in pMOE2, did not affect the open reading frame of *brkA* (Figure 4B). We believe that this is a meaningful indication that there should have been proper transcription and subsequent translation of *brkA* from pMOE1, pMOE2, and pMOE3. Furthermore, when the pMOE1, pMOE2, and pMOE3 sequences were aligned with pENS using MUSCLE (24), the DNA sequences perfectly aligned aside from the deleted regions and ScaI insertion sites (Figure 2C). This pairwise analysis revealed that there were no off-target mutations impacting DNA regions recognized by transcription or translation machinery. Taken together, these results indicate that it is unlikely that our manipulations of the *brkA* sequence impacted its transcription or translation.

Although this study achieved several important first steps towards generating relevant *brkA* constructs for the exploration of an entropy model of BrkA translocation, further investigation is required to determine why BrkA was not detected in any of our constructs. Alternatively, this study may serve as inspiration for new experimental strategies to evaluate the role of entropy in BrkA surface expression, as discussed in future directions.

Conclusions In this study, we investigated the driving force of passenger domain translocation and the optimization of 6xHis tag surface display from a unique autotransporter, BrkA. We created three plasmid constructs, pMOE1, pMOE2, and pMOE3, by engineering different passenger domain deletions and restriction enzyme site insertions using site directed mutagenesis. Through gel electrophoresis, restriction enzyme digestion and Nanopore sequencing, correct deletions and insertions in all three pMOEs were confirmed. *E. coli* UT5600 cells were transformed with the three plasmid constructs, but we were not able to detect BrkA expression by 6xHis tags from the transformants through Western blotting. Although several potential explanations for this failure to detect BrkA expression in pMOE1, pMOE2, and pMOE3 were explored, the cause remains unknown. However, we hope this initial exploration of the driving force behind BrkA translocation will serve as inspiration for future explorations of this unknown mechanism.

Future Directions Despite the generation of the pMOE1, pMOE2, and pMOE3 constructs, this study faced challenges in detection of the BrkA-associated 6xHis tag. Nevertheless, this investigation paves the way for future exploration into the proposed entropy model as the force driving BrkA passenger translocation. Future researchers could develop a more refined method for BrkA detection, which could allow them to make use of the pMOE constructs developed in this study to investigate the entropy model. More specifically, future groups could incorporate a novel 6xHis tag into readily accessible regions of the pMOE BrkA proteins, based on their predicted structural models (Figure 4A). Alternatively, they could explore the insertion of an exogenous sequence into the *brkA* passenger on pMOE1, pMOE2, and pMOE3, enabling detection through alternative assays, such as enzymatic reactions or epitope detection via Enzyme-Linked Immunosorbent Assay (ELISA). If this study were conducted, its findings could not only be used to assess the validity of the entropy model but also to evaluate the impact of passenger length on exogenous protein expression using the BrkA system.

ACKNOWLEDGEMENTS

We extend our gratitude toward Dr. David Oliver, Jade Muileboom and Virginie Jean-Baptiste, along with the entire MICB 471 teaching team for their support, mentorship and guidance throughout this research project. Additionally, we acknowledge the contribution of Goh et al. for providing the pENS plasmid for our study. Lastly, we express our appreciation to the Department of Microbiology and Immunology at the University of British Columbia for providing the necessary laboratory space, resources, and funding for this project.

CONTRIBUTIONS

MD: Collaborated with EM on results, discussion and supplemental materials, generated figures. Performed general manuscript editing and review.
OK: Composed the title, introduction, materials and methods, conclusion and references. Contributed to writing the abstract and future directions. Performed general manuscript editing and review.
EM: Collaborated with MD on results, discussion and supplemental materials, generated figures. Contributed to writing the abstract and future directions. Performed general manuscript editing and review.
All authors contributed to the design and conduction of all experiments, troubleshooting and final editing of the manuscript.

REFERENCES

1. **Green ER, Mecsas J.** 2016. Bacterial Secretion Systems: An Overview. Microbiol Spectr **4**.
2. **Fan E, Chauhan N, Udatha DBRKG, Leo JC, Linke D.** 2016. Type V Secretion Systems in Bacteria. Microbiol Spectr **4**:10.1128/microbiolspec.vmbf-0009–2015.
3. **Trivedi A, Gosai J, Nakane D, Shrivastava A.** 2022. Design Principles of the Rotary Type 9 Secretion System. Front Microbiol **13**:845563.
4. **Maphosa S, Moleleki LN, Motaung TE.** 2023. Bacterial secretion system functions: evidence of interactions and downstream implications. Microbiology **169**:001326.
5. **Dautin N.** 2021. Folding Control in the Path of Type 5 Secretion. Toxins **13**:341.
6. **Rambow AA, Fernandez RC, Weiss AA.** 1998. Characterization of BrkA Expression in *Bordetella bronchiseptica*. Infect Immun **66**:3978–3980.
7. **Raeven RHM, van Vlies N, Salverda MLM, van der Maas L, Uittenbogaard JP, Bindels THE, Rigters J, Verhagen LM, Kruijer S, van Riet E, Metz B, van der Ark AAJ.** 2020. The Role of Virulence Proteins in Protection Conferred by *Bordetella pertussis* Outer Membrane Vesicle Vaccines. Vaccines **8**:429.
8. **Barnes MG, Weiss AA.** 2001. BrkA Protein of *Bordetella pertussis* Inhibits the Classical Pathway of Complement after C1 Deposition. Infect Immun **69**:3067–3072.
9. **Meuskens I, Saragliadis A, Leo JC, Linke D.** 2019. Type V Secretion Systems: An Overview of Passenger Domain Functions. Front Microbiol **10**.
10. **Bernstein HD.** 2019. Type V Secretion in Gram-Negative Bacteria. EcoSal Plus **8**.
11. **Oliver DC, Huang G, Nodel E, Pleasance S, Fernandez RC.** 2003. A conserved region within the *Bordetella pertussis* autotransporter BrkA is necessary for folding of its passenger domain. Mol Microbiol **47**:1367–1383.
12. **Marr N, Oliver DC, Laurent V, Poolman J, Denoël P, Fernandez RC.** 2008. Protective activity of the *Bordetella pertussis* BrkA autotransporter in the murine lung colonization model. Vaccine **26**:4306–4311.
13. **Fischer W, Buhrdorf R, Gerland E, Haas R.** 2001. Outer membrane targeting of passenger proteins by the vacuolating cytotoxin autotransporter of Helicobacter pylori. Infect Immun **69**:6769–6775.
14. **Baclayon M, Ulsen P van, Mouhib H, Shabestari MH, Verzijden T, Abeln S, Roos WH, Wuite GJL.** 2016. Mechanical Unfolding of an Autotransporter Passenger Protein Reveals the Secretion Starting Point and Processive Transport Intermediates. ACS Nano **10**:5710–5719.
15. **Yuan X, Johnson MD, Zhang J, Lo AW, Schembri MA, Wijeyewickrema LC, Pike RN, Huysmans GHM, Henderson IR, Leyton DL.** 2018. Molecular basis for the folding of β-helical autotransporter passenger domains. 1. Nat Commun **9**:1395.
16. **Junker M, Schuster CC, McDonnell AV, Sorg KA, Finn MC, Berger B, Clark PL.** 2006. Pertactin β-helix folding mechanism suggests common themes for the secretion and folding of autotransporter proteins. Proc Natl Acad Sci **103**:4918–4923.
17. **Pang YT, Hazel AJ, Gumbart JC.** 2023. Uncovering the folding mechanism of pertactin: A comparative study of isolated and vectorial folding. Biophys J **122**:2988–2995.
18. **Sun F, Pang X, Xie T, Zhai Y, Wang G, Sun F.** 2015. BrkAutoDisplay: functional display of multiple exogenous proteins on the surface of Escherichia coli by using BrkA autotransporter. Microb Cell Factories **14**:129.
19. **Nicolay T, Vanderleyden J, Spaepen S.** 2015. Autotransporter-based cell surface display in Gram-negative bacteria. Crit Rev Microbiol **41**:109–123.
20. **Tu, A.** (2008). Transformation of Escherichia coli Made Competent by Calcium Chloride Protocol. *American Society for Microbiology*
21. **Sichwart S, Tozakidis IEP, Teese M, Jose J.** 2015. Maximized Autotransporter-Mediated Expression (MATE) for Surface Display and Secretion of Recombinant Proteins in Escherichia coli. Food Technol Biotechnol **53:**251–260.
22. **Gasteiger E, Gattiker A, Hoogland C, Ivanyi I, Appel RD, Bairoch A.** 2003. ExPASy: the proteomics server for in-depth protein knowledge and analysis. Nucleic Acids Res **31**:3784–3788.
23. **Schwede T, Kopp J, Guex N, Peitsch MC.** 2003. SWISS-MODEL: an automated protein homology-modeling server. Nucleic Acids Res **31**:3381–3385.

24. **Edgar RC.** 2004. MUSCLE: multiple sequence alignment with high accuracy and high throughput. Nucleic Acids Res **32:**1792–1797.